hep-ex/9705014 21 May 1997

Proton Dissociative ρ and Elastic ϕ Electroproduction at HERA

H1 Collaboration

Abstract

The electroproduction of ρ mesons with proton diffractive dissociation for $Q^2 > 7$ GeV^2 and the elastic electroproduction of ϕ mesons for $Q^2 > 6$ GeV^2 are studied in e^+p collisions at HERA with the H1 detector, for an integrated luminosity of 2.8 pb^{-1}. The dependence of the cross sections on P_t^2 and Q^2 is measured, and the vector meson polarisation obtained. The cross section ratio between proton dissociative and elastic production of ρ mesons is measured and discussed in the framework of the factorisation hypothesis of diffractive vertices. The ratio of the elastic cross section for ϕ and ρ meson production is investigated as a function of Q^2.
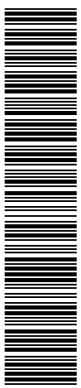
C. Adloff[35], S. Aid[13], M. Anderson[23], V. Andreev[26], B. Andrieu[29], V. Arkadov[36], C. Arndt[11], I. Ayyaz[30], A. Babaev[25], J. Bähr[36], J. Bán[18], P. Baranov[26], E. Barrelet[30], R. Barschke[11], W. Bartel[11], U. Bassler[30], H.P. Beck[38], M. Beck[14], H.-J. Behrend[11], A. Belousov[26], Ch. Berger[1], G. Bernardi[30], G. Bertrand-Coremans[4], R. Beyer[11], P. Biddulph[23], J.C. Bizot[28], K. Borras[8], F. Botterweck[27], V. Boudry[29], S. Bourov[25], A. Braemer[15], W. Braunschweig[1], V. Brisson[28], D.P. Brown[23], W. Brückner[14], P. Bruel[29], D. Bruncko[18], C. Brune[16], J. Bürger[11], F.W. Büsser[13], A. Buniatian[4], S. Burke[19], G. Buschhorn[27], D. Calvet[24], A.J. Campbell[11], T. Carli[27], M. Charlet[11], D. Clarke[5], B. Clerbaux[4], S. Cocks[20], J.G. Contreras[8], C. Cormack[20], J.A. Coughlan[5], M.-C. Cousinou[24], B.E. Cox[23], G. Cozzika[9], D.G. Cussans[5], J. Cvach[31], S. Dagoret[30], J.B. Dainton[20], W.D. Dau[17], K. Daum[40], M. David[9], C.L. Davis[19,41], A. De Roeck[11], E.A. De Wolf[4], B. Delcourt[28], M. Dirkmann[8], P. Dixon[19], W. Dlugosz[7], C. Dollfus[38], K.T. Donovan[21], J.D. Dowell[3], H.B. Dreis[2], A. Droutskoi[25], J. Ebert[35], T.R. Ebert[20], G. Eckerlin[11], V. Efremenko[25], S. Egli[38], R. Eichler[37], F. Eisele[15], E. Eisenhandler[21], E. Elsen[11], M. Erdmann[15], A.B. Fahr[13], L. Favart[28], A. Fedotov[25], R. Felst[11], J. Feltesse[9], J. Ferencei[18], F. Ferrarotto[33], K. Flamm[11], M. Fleischer[8], M. Flieser[27], G. Flügge[2], A. Fomenko[26], J. Formánek[32], J.M. Foster[23], G. Franke[11], E. Gabathuler[20], K. Gabathuler[34], F. Gaede[27], J. Garvey[3], J. Gayler[11], M. Gebauer[36], R. Gerhards[11], A. Glazov[36], L. Goerlich[6], N. Gogitidze[26], M. Goldberg[30], K. Golec-Biernat[6], B. Gonzalez-Pineiro[30], I. Gorelov[25], C. Grab[37], H. Grässler[2], T. Greenshaw[20], R.K. Griffiths[21], G. Grindhammer[27], A. Gruber[27], C. Gruber[17], T. Hadig[1], D. Haidt[11], L. Hajduk[6], T. Haller[14], M. Hampel[1], W.J. Haynes[5], B. Heinemann[11], G. Heinzelmann[13], R.C.W. Henderson[19], H. Henschel[36], I. Herynek[31], M.F. Hess[27], K. Hewitt[3], K.H. Hiller[36], C.D. Hilton[23], J. Hladký[31], M. Höppner[8], D. Hoffmann[11], T. Holtom[20], R. Horisberger[34], V.L. Hudgson[3], M. Hütte[8], M. Ibbotson[23], Ç. İşsever[8], H. Itterbeck[1], M. Jacquet[28], M. Jaffre[28], J. Janoth[16], D.M. Jansen[14], L. Jönsson[22], D.P. Johnson[4], H. Jung[22], P.I.P. Kalmus[21], M. Kander[11], D. Kant[21], U. Kathage[17], J. Katzy[15], H.H. Kaufmann[36], O. Kaufmann[15], M. Kausch[11], S. Kazarian[11], I.R. Kenyon[3], S. Kermiche[24], C. Keuker[1], C. Kiesling[27], M. Klein[36], C. Kleinwort[11], G. Knies[11], T. Köhler[1], J.H. Köhne[27], H. Kolanoski[39], S.D. Kolya[23], V. Korbel[11], P. Kostka[36], S.K. Kotelnikov[26], T. Krämerkämper[8], M.W. Krasny[6,30], H. Krehbiel[11], D. Krücker[27], A. Küpper[35], H. Küster[22], M. Kuhlen[27], T. Kurča[36], B. Laforge[9], M.P.J. Landon[21], W. Lange[36], U. Langenegger[37], A. Lebedev[26], F. Lehner[11], V. Lemaitre[11], S. Levonian[29], M. Lindstroem[22], F. Linsel[11], J. Lipinski[11], B. List[11], G. Lobo[28], G.C. Lopez[12], V. Lubimov[25], D. Lüke[8,11], L. Lytkin[14], N. Magnussen[35], H. Mahlke-Krüger[11], E. Malinovski[26], R. Maraček[18], P. Marage[4], J. Marks[15], R. Marshall[23], J. Martens[35], G. Martin[13], R. Martin[20], H.-U. Martyn[1], J. Martyniak[6], T. Mavroidis[21], S.J. Maxfield[20], S.J. McMahon[20], A. Mehta[5], K. Meier[16], P. Merkel[11], F. Metlica[14], A. Meyer[13], A. Meyer[11], H. Meyer[35], J. Meyer[11], P.-O. Meyer[2], A. Migliori[29], S. Mikocki[6], D. Milstead[20], J. Moeck[27], F. Moreau[29], J.V. Morris[5], E. Mroczko[6], D. Müller[38], K. Müller[11], P. Murín[18], V. Nagovizin[25], R. Nahnhauer[36], B. Naroska[13], Th. Naumann[36], I. Négri[24], P.R. Newman[3], D. Newton[19], H.K. Nguyen[30], T.C. Nicholls[3], F. Niebergall[13], C. Niebuhr[11], Ch. Niedzballa[1], H. Niggli[37], G. Nowak[6], T. Nunnemann[14], H. Oberlack[27], J.E. Olsson[11], D. Ozerov[25], P. Palmen[2], E. Panaro[11], A. Panitch[4], C. Pascaud[28], S. Passaggio[37], G.D. Patel[20], H. Pawletta[2], E. Peppel[36], E. Perez[9], J.P. Phillips[20],

A. Pieuchot[24], D. Pitzl[37], R. Pöschl[8], G. Pope[7], B. Povh[14], K. Rabbertz[1], P. Reimer[31], H. Rick[8], S. Riess[13], E. Rizvi[21], P. Robmann[38], R. Roosen[4], K. Rosenbauer[1], A. Rostovtsev[30], F. Rouse[7], C. Royon[9], K. Rüter[27], S. Rusakov[26], K. Rybicki[6], D.P.C. Sankey[5], P. Schacht[27], S. Schiek[11], S. Schleif[16], P. Schleper[15], W. von Schlippe[21], D. Schmidt[35], G. Schmidt[11], L. Schoeffel[9], A. Schöning[11], V. Schröder[11], E. Schuhmann[27], B. Schwab[15], F. Sefkow[38], A. Semenov[25], V. Shekelyan[11], I. Sheviakov[26], L.N. Shtarkov[26], G. Siegmon[17], U. Siewert[17], Y. Sirois[29], I.O. Skillicorn[10], T. Sloan[19], P. Smirnov[26], M. Smith[20], V. Solochenko[25], Y. Soloviev[26], A. Specka[29], J. Spiekermann[8], S. Spielman[29], H. Spitzer[13], F. Squinabol[28], P. Steffen[11], R. Steinberg[2], J. Steinhart[13], B. Stella[33], A. Stellberger[16], J. Stiewe[16], U. Stößlein[36], K. Stolze[36], U. Straumann[15], W. Struczinski[2], J.P. Sutton[3], S. Tapprogge[16], M. Taševský[32], V. Tchernyshov[25], S. Tchetchelnitski[25], J. Theissen[2], G. Thompson[21], P.D. Thompson[3], N. Tobien[11], R. Todenhagen[14], P. Truöl[38], G. Tsipolitis[37], J. Turnau[6], E. Tzamariudaki[11], P. Uelkes[2], A. Usik[26], S. Valkár[32], A. Valkárová[32], C. Vallée[24], P. Van Esch[4], P. Van Mechelen[4], D. Vandenplas[29], Y. Vazdik[26], P. Verrecchia[9], G. Villet[9], K. Wacker[8], A. Wagener[2], M. Wagener[34], R. Wallny[15], T. Walter[38], B. Waugh[23], G. Weber[13], M. Weber[16], D. Wegener[8], A. Wegner[27], T. Wengler[15], M. Werner[15], L.R. West[3], S. Wiesand[35], T. Wilksen[11], S. Willard[7], M. Winde[36], G.-G. Winter[11], C. Wittek[13], M. Wobisch[2], H. Wollatz[11], E. Wünsch[11], J. Žáček[32], D. Zarbock[12], Z. Zhang[28], A. Zhokin[25], P. Zini[30], F. Zomer[28], J. Zsembery[9], and M. zurNedden[38],

[1] I. Physikalisches Institut der RWTH, Aachen, Germany[a]
[2] III. Physikalisches Institut der RWTH, Aachen, Germany[a]
[3] School of Physics and Space Research, University of Birmingham, Birmingham, UK[b]
[4] Inter-University Institute for High Energies ULB-VUB, Brussels; Universitaire Instelling Antwerpen, Wilrijk; Belgium[c]
[5] Rutherford Appleton Laboratory, Chilton, Didcot, UK[b]
[6] Institute for Nuclear Physics, Cracow, Poland[d]
[7] Physics Department and IIRPA, University of California, Davis, California, USA[e]
[8] Institut für Physik, Universität Dortmund, Dortmund, Germany[a]
[9] CEA, DSM/DAPNIA, CE-Saclay, Gif-sur-Yvette, France
[10] Department of Physics and Astronomy, University of Glasgow, Glasgow, UK[b]
[11] DESY, Hamburg, Germany[a]
[12] I. Institut für Experimentalphysik, Universität Hamburg, Hamburg, Germany[a]
[13] II. Institut für Experimentalphysik, Universität Hamburg, Hamburg, Germany[a]
[14] Max-Planck-Institut für Kernphysik, Heidelberg, Germany[a]
[15] Physikalisches Institut, Universität Heidelberg, Heidelberg, Germany[a]
[16] Institut für Hochenergiephysik, Universität Heidelberg, Heidelberg, Germany[a]
[17] Institut für Reine und Angewandte Kernphysik, Universität Kiel, Kiel, Germany[a]
[18] Institute of Experimental Physics, Slovak Academy of Sciences, Košice, Slovak Republic[f,j]
[19] School of Physics and Chemistry, University of Lancaster, Lancaster, UK[b]
[20] Department of Physics, University of Liverpool, Liverpool, UK[b]
[21] Queen Mary and Westfield College, London, UK[b]
[22] Physics Department, University of Lund, Lund, Sweden[g]
[23] Physics Department, University of Manchester, Manchester, UK[b]
[24] CPPM, Université d'Aix-Marseille II, IN2P3-CNRS, Marseille, France
[25] Institute for Theoretical and Experimental Physics, Moscow, Russia
[26] Lebedev Physical Institute, Moscow, Russia[f]
[27] Max-Planck-Institut für Physik, München, Germany[a]

[28] LAL, Université de Paris-Sud, IN2P3-CNRS, Orsay, France

[29] LPNHE, Ecole Polytechnique, IN2P3-CNRS, Palaiseau, France

[30] LPNHE, Universités Paris VI and VII, IN2P3-CNRS, Paris, France

[31] Institute of Physics, Czech Academy of Sciences, Praha, Czech Republic[f,h]

[32] Nuclear Center, Charles University, Praha, Czech Republic[f,h]

[33] INFN Roma 1 and Dipartimento di Fisica, Università Roma 3, Roma, Italy

[34] Paul Scherrer Institut, Villigen, Switzerland

[35] Fachbereich Physik, Bergische Universität Gesamthochschule Wuppertal, Wuppertal, Germany[a]

[36] DESY, Institut für Hochenergiephysik, Zeuthen, Germany[a]

[37] Institut für Teilchenphysik, ETH, Zürich, Switzerland[i]

[38] Physik-Institut der Universität Zürich, Zürich, Switzerland[i]

[39] Institut für Physik, Humboldt-Universität, Berlin, Germany[a]

[40] Rechenzentrum, Bergische Universität Gesamthochschule Wuppertal, Wuppertal, Germany[a]

[41] Visitor from Physics Dept. University Louisville, USA

1 Introduction

Vector meson production in lepton-proton collisions is a powerful probe for investigating the nature of diffraction. At HERA, because of the wide kinematic range accessible in W, the photon-proton centre of mass energy, and in Q^2, the photon virtuality [1], detailed information on the mechanism of the diffractive process can be accumulated. The opportunity to study the production of vector mesons with different quark contents (ρ,ϕ) in the elastic and proton dissociation channels adds further to the information.

Many experimental results on elastic ρ, ω, ϕ and J/ψ meson production by quasi-real photons ($Q^2 \approx 0$) [1,2,3,4,5,6] and virtual photons ($Q^2 \gtrsim 7$ GeV^2) [7,8,9] have been obtained by the H1 and ZEUS experiments. Also numerous elastic vector meson production data have been reported by fixed target experiments [10,11,12,13] at lower W, providing information about the energy behaviour of vector meson production. However, little is known about the vector meson proton dissociative process. In the H1 experiment, the use of the forward detectors (see Sect.2) makes it possible to separate efficiently the proton elastic from the proton dissociative channels and has led to the first results on proton dissociative J/ψ photoproduction [2]. As yet, no data exist in the high Q^2 region. This contrasts with the situation at high energy proton colliders, where the proton diffractive dissociation process $pp \to pY$ has been widely investigated [14,15,16,17].

Different theoretical models have been proposed in order to describe diffractive vector meson production. In the framework of Regge theory [18], which successfully relates many features of hadronic interactions, diffractive vector meson production is described using the Vector Dominance Model (VDM) [19,20]. Several QCD models describe diffraction as an exchange of a two gluon system [21] adopting either a non-perturbative [22,23] or a perturbative approach. In the latter case, either different variants of a constituent quark model [24,25,26,27] or a leading order logarithmic approximation have been used [28,29,30]. These models lead to different predictions for the centre of mass energy dependence of the γ^*p cross section. In the non-perturbative case it is "soft", i.e. similar to that measured in elastic hadron-hadron scattering, while for the perturbative calculations a rapid increase of the cross section with W is obtained due to the rise of the gluon distribution in the proton in the low Bjorken-x region. All calculations predict a similar Q^{-6} behaviour for the γ^*p cross section, which in the perturbative approach may be modified to account for the evolution of the parton distributions and quark Fermi motion [30,31]. At high Q^2 the vector mesons are expected to be mostly longitudinally polarised [23].

The first part of the paper presents the first results on ρ meson production with proton dissociation for $Q^2 > 7$ GeV^2. The cross section ratio for proton dissociative to elastic ρ production, which is less sensitive to theoretical and experimental uncertainties than absolute cross section values, is measured in four intervals of W and Q^2. The Q^2 dependence and polarisation are determined for the proton dissociation process. The second part of the paper presents data on elastic ϕ meson production, with emphasis on the Q^2 evolution of the cross section ratio of elastic ϕ to elastic ρ production.

---

[1] Q^2 is the negative square of the four-momentum transfer from the initial to the final state lepton.

2   H1 Detector and Event Selection

The data correspond to an integrated luminosity of 2.8 pb^{-1}. They were collected in 1994, when the HERA collider was operated with positrons of 27.5 GeV interacting with protons of 820 GeV. The H1 detector is described in detail in [32]. As the event selection in both analyses presented have many features in common, they will be treated together in this section. Analysis specific cuts will be addressed in the appropriate sections.

The basic event topology selected for both analyses consists of a positron recorded in the backward electromagnetic calorimeter (BEMC) and two oppositely charged particles, originating from a vertex situated in the nominal e^+p interaction region which are detected in the tracking system. The detectors placed in the forward region of the H1 detector [2] are used to distinguish between elastic and proton dissociation events.

The positron is identified as an electromagnetic cluster with an energy larger than 12 GeV, which is reconstructed in the BEMC and to which a hit in the backward multiwire proportional chamber (BPC) is associated. The polar angle of the scattered positron θ is determined from the position of the BPC hit closest to the BEMC cluster and the position of the interaction vertex. The trigger used to collect the present data required a total deposited energy in the BEMC larger than 8 GeV outside a square of 32×32 cm^2 around the beam pipe.

Two tracks are required to be detected in the central tracking system, which are assumed to be pions from the ρ meson decay or kaons from the ϕ meson decay. To be accepted, tracks must be reconstructed from at least 5 hits in the drift chambers and have a transverse momentum larger than 0.1 GeV/c. Except for the positron track and the tracks related to the vector meson decay products, no other tracks in the polar angular range of $5° < \theta < 170°$ are allowed.

The central tracking detector is surrounded by the liquid argon calorimeter (LAr). In the ρ analysis, in order to suppress the background, events including clusters with energies in the LAr or BEMC exceeding 0.5 GeV and 1.0 GeV respectively, other than those associated with the scattered positron or vector meson decay products, are rejected. However clusters with a pseudorapidity $\eta > 2.5$ [3] are allowed, as they can be due to particles originating from the decay of the proton dissociative system. In the analysis of ϕ meson elastic production, it is required that the energy deposition in the forward part of the LAr with $\eta > 2$ should be smaller than 1.0 GeV.

Proton dissociation events are tagged by the three following subdetectors: the forward part ($\eta > 2.5$) of the LAr calorimeter, the forward muon detector (FMD) and the proton remnant tagger (PRT). These subdetectors are sensitive to particles either directly emitted from the dissociative proton system or rescattered in the beam pipe wall or material close to the beam pipe and thus allow the detection of primary particles with pseudorapidities up to ~ 7.5. In order to tag proton dissociative events it is required that there be at least one of the following signals: a cluster with energy larger than 0.5 GeV in the forward part of the LAr calorimeter or two pairs of hits in the FMD or one hit in the PRT. For elastic events the absence of any signal in all three subdetectors is required.

---

[2]In the H1 coordinate system, the direction of the positive z axis coincides with the direction of the proton beam, defining the "forward" region. The polar angle is defined relative to the z axis.

[3]The pseudorapidity, $\eta = -\ln \tan \theta/2$, is positive in the forward region; θ is the polar angle.

In the ρ analysis, an "anti-ϕ" cut is applied to suppress the contamination of ϕ mesons: the invariant mass of the two detected particles, assumed to be kaons, is required to be larger than 1.05 GeV/c^2. This cut also reduces the background contribution from ω mesons.

To achieve the best accuracy in the determination of the kinematical variables the "double angle" method [33] is applied. With this method the precisely measured polar angles of the scattered positron and of the produced vector meson are used to compute the other kinematical variables.

3 Electroproduction of ρ Mesons with Proton Dissociation

3.1 Diffractive Dissociation and Factorisation

Elastic and proton dissociative ρ meson electroproduction are illustrated in Fig.1a and 1b respectively, where Y is a low mass system resulting from the proton diffractive dissociation.
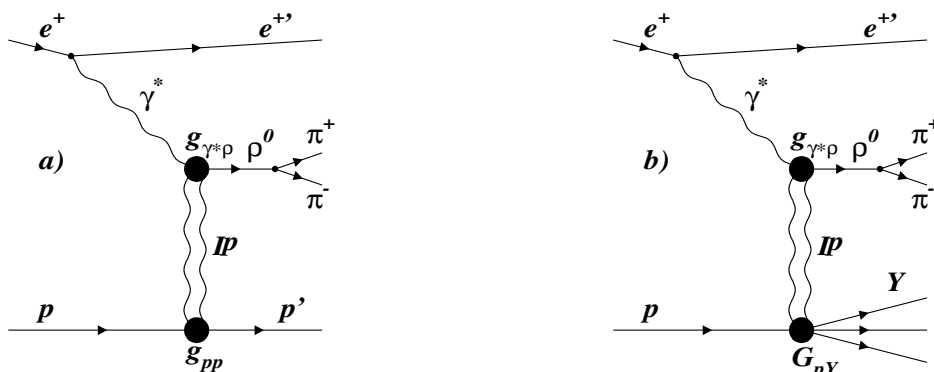
Figure 1: Diffractive ρ meson production: a) elastic scattering; b) proton dissociation.

The hypothesis of factorisation of the diffractive vertex [34, 35, 36] naturally appears in the framework of Regge theory assuming a single pomeron exchange. It implies that each amplitude is proportional to the product of two vertex functions. The differential cross section ratio of proton diffractive dissociation to elastic scattering can be expressed (see Fig. 1) as

$$\frac{\mathrm{d}^2\sigma_{pdis}/\mathrm{d}t\,\mathrm{d}M_Y^2}{\mathrm{d}\sigma_{el}/\mathrm{d}t} \propto \left(\frac{\mathrm{g}_{\gamma^*\rho}(t,Q^2,\lambda)\,\mathrm{G}_{pY}(t,M_Y)}{\mathrm{g}_{\gamma^*\rho}(t,Q^2,\lambda)\,\mathrm{g}_{pp}(t)} \right)^2 = f(t,M_Y), \tag{1}$$

where M_Y is the mass of the proton dissociative system, $t = (P_p - P_{p'(Y)})^2$ the square of the four-momentum transfer from the initial to the final state proton (or dissociative system Y), λ the helicity state of the ρ meson and $\mathrm{g}_{\gamma^*\rho}$, g_{pp} and G_{pY} the vertex functions. The vertex function G_{pY} can be calculated using a triple-Regge vertex approach [34] for

M_Y well in excess of the proton mass. The vertex function $g_{\gamma^*\rho}$ cancels in eq. (1) and the cross section ratio depends only on t and M_Y. Hence at fixed t, the elastic process and the proton dissociative process, independently of M_Y, should exhibit a similar Q^2 dependence and lead to similar vector meson polarisation.

Other exchange schemes, besides single pomeron exchange, may lead to a deviation from factorisation. Deviations due to the contribution of sub-leading reggeon exchanges or two-pomeron exchange have been estimated to be of the order of $\sim 30\%$ or less (see [34] and references therein).

A basic feature of the diffractive processes is an exponential fall $d\sigma/dt \propto e^{-b|t|}$ of the cross section in the low $|t|$ region. In the Regge approach the proton dissociative slope of the diffractive peak varies as a function of W and M_Y :

$$b(W, M_Y) = b_0 + 2\alpha' \ln(W^2/M_Y^2), \qquad (2)$$

where the constant b_0 can be decomposed as a sum of two contributions, which define the t-dependences of the $\gamma^*\rho$ and triple-pomeron vertices. The parameter α' is the slope of the pomeron trajectory, approximately equal to $0.25\,\mathrm{GeV}^{-2}$ [37], as deduced from hadron-hadron interaction measurements. The effective b-slope of the triple-pomeron vertex is measured to be approximately 1 GeV^{-2} [38]. Consequently it is expected that at high Q^2 the proton dissociative b-slope is considerably smaller then the elastic one, the latter reflecting the influence of the size of the proton. It has to be noted that, for QCD inspired models, the b-slope of the diffractive peak at high Q^2 is sometimes assumed to be essentially independent of the total energy W [30], but this is not a prediction of all models [25].

In a naive additive quark model the proton dissociative process is treated as a quasi-elastic scattering off the constituent quark in the proton, while the elastic process is treated as a coherent scattering off the proton [39]. This approach also predicts a considerable difference between the elastic and proton dissociative b-slopes.

A detailed experimental study of the proton dissociative $pp \to pY$ process was performed in several proton collider experiments [14,15,16,17]. The differential cross section $d\sigma/dM_Y^2$ exhibits an approximate $1/M_Y^2$ dependence. For large M_Y, the slope parameter b is approximately independent of M_Y, but with decreasing M_Y it increases according to eq. (2) and even more steeply for very low masses [14]. The factorisation hypothesis was found to be satisfied to within $\sim 20\%$ in low energy fixed target experiments [38] up to the ISR collider energies [40]. However the proton dissociation cross section rises unexpectedly slowly with increasing energy at the SPS and Tevatron colliders, which can be interpreted as a deviation from factorisation [14,15].

3.2   Kinematic Selections, Efficiencies and Backgrounds

In addition to the selection criteria discussed in section 2, the kinematic region in this analysis is restricted to:

$$7 \; < \; Q^2 \; < \; 35\ \mathrm{GeV}^2, \quad 60 \; < \; W \; < \; 180\ \mathrm{GeV}. \qquad (3)$$

The measured reaction is $\gamma^*p \to \rho Y$, where $M_Y^2/W^2 < 0.05$. Although M_Y^2 is not measured explicitly, the M_Y^2/W^2 range of the measurement is limited by the forward

detector selection criteria. The system Y carries most of the momentum of the incoming proton and is separated from the ρ meson by a large rapidity gap.

Such events are modelled by the Monte Carlo (MC) generator, DIFFVM [41], which, together with a detailed simulation of the H1 detector, is used to study efficiencies. Details of the simulation of the dissociated proton system are presented in [2]. The events are generated with an M_Y^2 distribution proportional to $1/M_Y^{2n}$ with $n=1.1$ for excited masses above 4 GeV/c^2. Below 4 GeV/c^2 the mass distribution is taken to follow diffractive dissociation data obtained from measurements of proton-deuterium interactions [35]. A systematic uncertainty in the detection efficiency is estimated by varying the parameter n in the $1/M_Y^{2n}$ distribution from 0.9 to 1.3 and by using different models for the fragmentation of the dissociative proton system. This systematic uncertainty is found to be $\sim 7\%$ and conservatively reflects a model dependence of the forward detection efficiency determination for the kinematic region $M_Y^2/W^2 < 0.05$. A possible proton resonance contribution at low M_Y^2 [35] and possible sub-leading exchange contributions in the larger M_Y^2 region [34] are encompassed in the above variations of the parameter n. In the very low M_Y region the forward detection efficiency decreases with decreasing M_Y, falling to below 50 % for $M_Y < 1.6$ GeV/c^2.

To estimate the accuracy with which the MC can reproduce the forward detector efficiencies, the relative tagging probabilities of proton dissociation events by the different forward subdetectors obtained by MC are compared with those from the data. These comparisons show that the MC determination of the forward detection efficiencies has an accuracy of $\sim 7\%$. The uncertainty arising from statistical fluctuations in the MC efficiency determination is $\sim 2\%$.

The background results from the elastic ρ meson production reaction, $\gamma^* p \to \rho p$, and the $\gamma^* p \to \rho Y$ reaction where $M_Y^2/W^2 > 0.05$. The latter events survive the selection criteria when at least one particle with $\eta < 2.5$ has not been observed in the detector. This background is further suppressed by two additional cuts:

$$P_t^2 < 0.8 \text{ GeV}^2, \quad \sum (E - P_z) > 53 \text{ GeV}, \tag{4}$$

where P_t^2 is the square of the vectorial sum of the momenta of the electron and pions transverse to the beam direction [4] and the sum is taken over the energy and momentum of the pions from the ρ meson decay and the scattered positron, computed with the "double angle" method.

Elastic ρ events survive the dissociative selection requirements when either the elastic proton strikes the beam pipe and is detected in the PRT, or when there is noise in at least one of the forward detectors: the forward region of the LAr, the FMD or the PRT. The probability of the proton being detected in the PRT is estimated using the DIFFVM MC generator and found to be $1.0 \pm 0.3\%$. The fraction of elastic events with noise in the forward detectors which would lead to them being identified as proton dissociative is found by studying events from random triggers. For the forward region of the LAr the fraction is $1.0 \pm 0.2\%$, for the FMD $3.0 \pm 1.5\%$ and for the PRT $\sim 0.1\%$.

The non-elastic background can be expected from processes of a non-diffractive deep inelastic scattering (DIS) or double (proton and photon) dissociative (DD) nature, which

---

[4]At HERA energies $P_t^2 \simeq |t|$. For diffractive vector meson events, P_t^2 is equal to the transverse momentum of the scattered proton or dissociative proton system.

8

also account for the non-resonant contribution under the ρ signal. Such events are studied in the high P_t^2 region or using a sidebands method and are found to have a shallow P_t^2 distribution, corresponding to a b-slope value of $0.2 \pm 0.1\,\mathrm{GeV}^{-2}$. Therefore, events surviving the selection cuts but with $P_t^2 > 2.0\,\mathrm{GeV}^2$, where the signal event contribution is expected to be negligible, are used to estimate the background level. Extrapolating this level to the $P_t^2 < 0.8\,\mathrm{GeV}^2$ region, using the b value obtained above, yields an expected non-elastic contribution of $12 \pm 6\%$ in the mass interval $0.6 < M_{\pi^+\pi^-} < 1.0$ GeV/c^2. Included in the $12\pm6\%$ there is a $3\pm3\%$ resonant background part (i.e. part producing a ρ peak), which is obtained from a fit to the mass distribution of the events at $P_t^2 > 2.0\,\mathrm{GeV}^2$. The level of the non-resonant contribution found by this method and obtained from the fit of the $\pi^+\pi^-$ mass spectrum (section 3.3) are in good agreement.

Using the DIFFVM MC, the background contribution from proton dissociative electroproduction of ϕ and ω mesons is estimated to be smaller than 1% after applying the "anti-ϕ" cut. The effects of QED photon radiation are simulated by the HERACLES 4.4 generator [42] and a corresponding correction of $4 \pm 3\%$ is applied.

3.3   Mass and P_t^2 Distributions

The invariant $\pi^+\pi^-$ mass spectrum of the proton dissociative data sample is shown in Fig. 2a for the kinematical region $P_t^2 < 0.8\,\mathrm{GeV}^2$. A prominent peak is observed at the nominal ρ meson mass position. The $\pi^+\pi^-$ mass spectrum is fitted with a relativistic Breit-Wigner function [43] with a P-wave energy dependent width to describe the ρ meson signal and a second order polynomial to describe the non-resonant background. With the ρ mass and width fixed to the nominal values [44], the fit gives 101 ± 13 events corresponding to the ρ meson signal. The systematic error, evaluated by varying the parameterisations of the signal and background shapes (see [7]), is found to be $\sim 8\%$. Smearing effects due to detector resolution are estimated using a Monte Carlo simulation and the distortion of the ρ meson signal shape is found to be negligibly small.

The acceptance corrected P_t^2 distribution is shown in Fig. 2b for the selected events for which the $\pi^+\pi^-$ invariant mass is in the interval $0.6 < M_{\pi^+\pi^-} < 1.0\,\mathrm{GeV}/\mathrm{c}^2$. To extract the exponential slope parameter, the backgrounds are estimated and subtracted in the fit. The background from elastically produced ρ mesons is evaluated using the above given MC estimates and taking into account the ratio of proton dissociative to elastic events. An exponential behaviour $e^{-b_{el}P_t^2}$ with $b_{el} = 7.0 \pm 0.8 \pm 0.6\,\mathrm{GeV}^{-2}$ [7] has been assumed. The shape of the P_t^2 distribution for the elastic events, in which the proton is detected in the PRT detector, is obtained from MC. The non-resonant $\pi^+\pi^-$ background is parameterised with $b_{bg} = 0.2 \pm 0.1\,\mathrm{GeV}^{-2}$, as outlined above.

With the background contributions fixed, the exponential slope parameter b_{pdis} is extracted from a fit to the overall P_t^2 spectrum assuming an exponential $e^{-b_{pdis}P_t^2}$ dependence of the proton dissociation cross section. A fit in the region $P_t^2 < 1.2\,\mathrm{GeV}^2$ yields a value of $b_{pdis} = 2.1 \pm 0.5\,(stat.) \pm 0.5\,(syst.)\,\mathrm{GeV}^{-2}$, where b_{pdis} is the average over all accessible M_Y values. The systematic uncertainty is due to the background subtraction and fit procedure. The uncertainty in the background subtraction is estimated by varying the background contributions and slopes within errors. The uncertainty in the fit procedure is estimated by varying the bin sizes, the bin positions and P_t^2 interval for the fit.
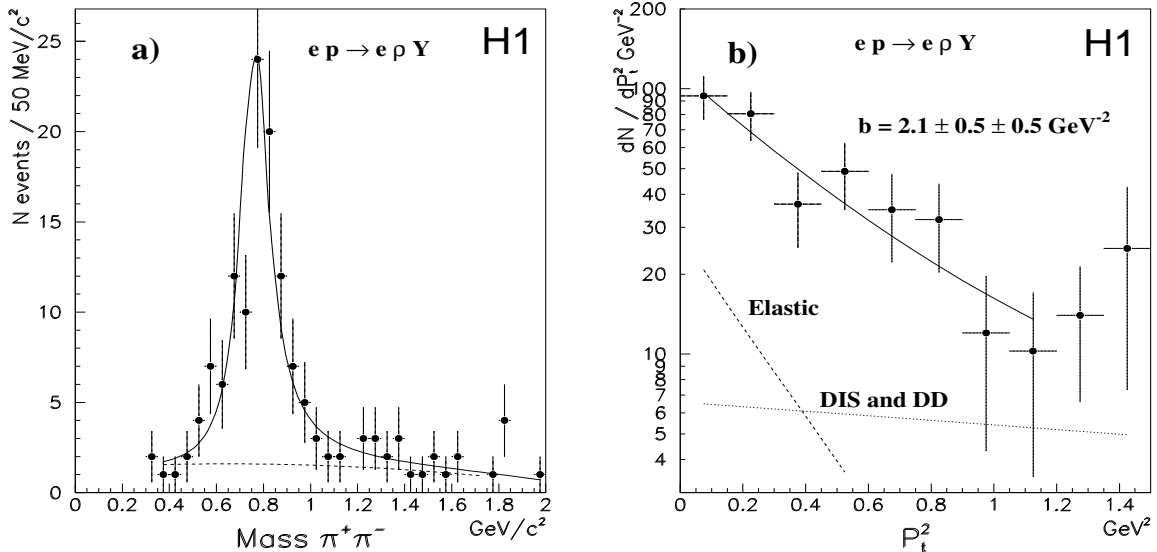
Figure 2: a) The invariant $\pi^+\pi^-$ mass spectrum for the kinematical region $P_t^2 < 0.8\,\mathrm{GeV}^2$. The solid curve represents the fit described in the text. The dashed curve shows the non-resonant background contribution. b) The efficiency corrected P_t^2 distribution for the proton dissociative data sample. The solid line represents the fit to the overall distribution, with the elastic (dotted line), DD and DIS (dashed line) contributions fixed (see text). Only statistical errors are presented.

The relatively small b-slope value for the proton dissociative channel indicates that both the $\gamma^*\rho$ and pY vertex functions (see Fig.1b) are characterised by small spatial dimensions, in contrast to the elastic scattering, where the pp vertex function corresponds to a value of $\sim 4 - 5\,\mathrm{GeV}^{-2}$. The measured b-slope value is close to the value obtained in proton dissociative J/ψ photoproduction, where $b = 1.6 \pm 0.3 \pm 0.1\,\mathrm{GeV}^{-2}$ [2], and to that obtained in double dissociative proton-proton scattering, where the b-slope tends to a value of $b_{DD} \sim 1.9\,\mathrm{GeV}^{-2}$ with increasing diffractive masses [40]. It implies that the contributions of the $\gamma^*\rho$, $\gamma J/\psi$ and pY vertex functions to the b-slopes are of the order of $1\,\mathrm{GeV}^{-2}$ or less.

The proton dissociative b-slope is expected to decrease with increasing M_Y according to eq. (2) and even faster in the low M_Y region. Such a behaviour was observed in proton-antiproton collider experiments [14], but has to be tested experimentally for the γ^*p process in the high Q^2 region. To investigate a possible M_Y mass dependence, the event sample is divided into two subsamples: a high M_Y subsample ($\langle M_Y \rangle \approx 6.8\,\mathrm{GeV}/c^2$), in which a cluster is detected in the forward part of the LAr calorimeter, and a low M_Y subsample ($\langle M_Y \rangle \approx 2.9\,\mathrm{GeV}/c^2$), characterised by the absence of clusters in the forward part of the LAr calorimeter. The values obtained for the b-slopes of the two event samples are $b_{high} = 2.7 \pm 1.3 \pm 0.7\,\mathrm{GeV}^{-2}$ and $b_{low} = 1.8 \pm 0.6 \pm 0.6\,\mathrm{GeV}^{-2}$, respectively. No evidence for any M_Y dependence of the b-slope is thus observed beyond the uncertainties of the measurement. It should be noted that low mass $M_Y < 1.6\,\mathrm{GeV}/c^2$ proton dissociative events cannot be efficiently tagged by the forward detectors.

3.4 Proton Dissociative to Elastic Cross Section Ratio

The ratio of the proton dissociative to the elastic ρ production cross section is calculated using the fit results obtained as described above and restricted to the kinematic region $7 < Q^2 < 35$ GeV^2 and $60 < W < 180$ GeV. The proton dissociative cross section corresponds to the region $M_Y^2/W^2 < 0.05$. Efficiency and acceptance corrections for the two event samples, the proton dissociative and elastic ρ events, are given in Table 1.

	Proton dissociation	Elastic scattering	Ratio, corrections
Number of events	101 ± 13	291 ± 23	0.35 ± 0.05
Trigger efficiencies	0.99 ± 0.01	0.99 ± 0.01	1.00
Selection efficiencies	0.39 ± 0.04	0.57 ± 0.02	1.46 ± 0.15
P_t^2 acceptance correction	1.23 ± 0.15	1.00 ± 0.01	1.23 ± 0.15
Forward detectors off	1.10 ± 0.01	0.97 ± 0.01	1.13 ± 0.02
Fit procedure	1.00 ± 0.08	1.00 ± 0.08	1.00 ± 0.05
Radiative corrections	0.96 ± 0.03	0.96 ± 0.03	1.00
Total background correction (a+b+c)	0.82 ± 0.07	0.89 ± 0.08	0.92 ± 0.11
a) Elastic background	0.15 ± 0.06		
b) Proton dissociation background		0.09 ± 0.08	
c) DD and DIS resonant background	0.03 ± 0.03	0.02 ± 0.01	

Table 1: Numbers of events, efficiencies and correction factors for the proton diffractive dissociation and the elastic scattering data samples.

The background contributions were discussed in section 3.2 and in [7]. The entry in Table 1 "Forward detectors off" corrects for some data taking periods, during which the FMD or PRT subdetectors were not operational. A systematic uncertainty in the luminosity measurement of $\sim 2\%$ cancels in the cross section ratio.

The cross section ratio is corrected for the P_t^2 acceptances using the exponential P_t^2 dependences and taking into account the uncertainty of the slope measurement. Some of the systematic uncertainties in the two event samples are not independent and therefore totally or partially cancel in the cross section ratio, as can be seen from Table 1.

The ratio of the proton dissociative to the elastic ρ meson production cross section is measured to be:

$$\frac{\sigma(ep \to e\rho Y)}{\sigma(ep \to e\rho p)} = 0.65 \pm 0.11(stat.) \pm 0.13(syst.). \tag{5}$$

The systematic error is dominated by the acceptance determinations, the background estimates and the fit procedure.

The ρ meson electroproduction cross section is converted into a $\gamma^* p$ cross section using the relation

$$\sigma(\gamma^* p \to \rho Y) = \frac{1}{\Gamma_T} \frac{\mathrm{d}^2\sigma(ep \to e\rho Y)}{\mathrm{d}W\,\mathrm{d}Q^2} \ , \quad \Gamma_T = \frac{\alpha_{em}}{\pi} \frac{(1 + (1-y)^2)}{W\,Q^2} \ , \tag{6}$$

where y is the Bjorken inelasticity variable, $\sigma(\gamma^*p \to \rho Y)$ the virtual photon-proton cross section and Γ_T the transverse virtual photon flux factor. The error on the Γ_T factor is estimated by varying the W or Q^2 distributions within errors, leading to an uncertainty in Γ_T of $\sim 7\%$. To study any dependence of the ratio on Q^2 and W, the data are divided in four (Q^2, W) bins. The proton dissociative $\sigma(\gamma^*p \to \rho Y)$ cross sections and ratios of the proton dissociative to the elastic cross sections for four kinematic intervals are presented in Table 2. Within uncertainties, no dependence of the cross section ratio on W or Q^2 is observed.

	$7 < Q^2 < 35\,\mathrm{GeV}^2$	
	$60 < W < 180$ GeV	
$\dfrac{\sigma(\gamma^*p \to \rho Y)}{\sigma(\gamma^*p \to \rho p)}$	$0.65 \pm 0.11 \pm 0.13$	
	$7 < Q^2 < 15\,\mathrm{GeV}^2$	
	$60 < W < 120$ GeV	$120 < W < 180$ GeV
$\sigma(\gamma^*p \to \rho Y)$ (nb)	$24 \pm 5 \pm 6$	$19 \pm 6 \pm 5$
$\dfrac{\sigma(\gamma^*p \to \rho Y)}{\sigma(\gamma^*p \to \rho p)}$	$0.74 \pm 0.17 \pm 0.16$	$0.63 \pm 0.22 \pm 0.14$
	$15 < Q^2 < 35\,\mathrm{GeV}^2$	
	$60 < W < 120$ GeV	$120 < W < 180$ GeV
$\sigma(\gamma^*p \to \rho Y)$ (nb)	$3.0 \pm 1.1 \pm 0.8$	$3.0 \pm 1.6 \pm 0.8$
$\dfrac{\sigma(\gamma^*p \to \rho Y)}{\sigma(\gamma^*p \to \rho p)}$	$0.60 \pm 0.26 \pm 0.14$	$0.51 \pm 0.31 \pm 0.13$

Table 2: The proton dissociative $\sigma(\gamma^*p \to \rho Y)$ cross sections and ratios of the proton dissociative to the elastic cross sections for four kinematic intervals.

3.5 Q^2 Dependence and Polarisation

The proton dissociative data in the region $0.6 < M_{\pi^+\pi^-} < 1.0\,\mathrm{GeV}/\mathrm{c}^2$ are used for the measurements of the γ^*p cross section Q^2 dependence and ρ polarisation. The background in the Q^2 distributions from elastic and from double dissociative and non-diffractive deep inelastic scattering are assumed to have a Q^{-n} behaviour with n values respectively $n = 5.0 \pm 1.0 \pm 0.4$ (see [7]) and $n = 3.0 \pm 0.5$, as obtained from a dedicated background study. The background subtracted Q^2 distribution for the reaction $\gamma^*p \to \rho Y$ (Fig. 3a) is well fitted by a Q^{-n} dependence with $n = 5.8 \pm 1.1 \pm 0.8$. The systematic error comes mainly from the uncertainties in the background subtraction, the fit procedure and the photon flux estimate. The Q^2 dependence is similar to that measured in elastic electro-production [7,8].

Information about the ρ meson polarisation can be extracted from the $\cos\vartheta^*$ angular distribution, where ϑ^* is the angle in the ρ meson rest frame between the direction of the π^+ and the direction of the ρ meson in the γ^*p center of mass system. This distribution is expected to be different for the different helicity states : $\propto \cos^2\vartheta^*$ for longitudinally polarised ρ mesons and $\propto \sin^2\vartheta^*$ for transversely polarised ρ mesons. Explicitly the
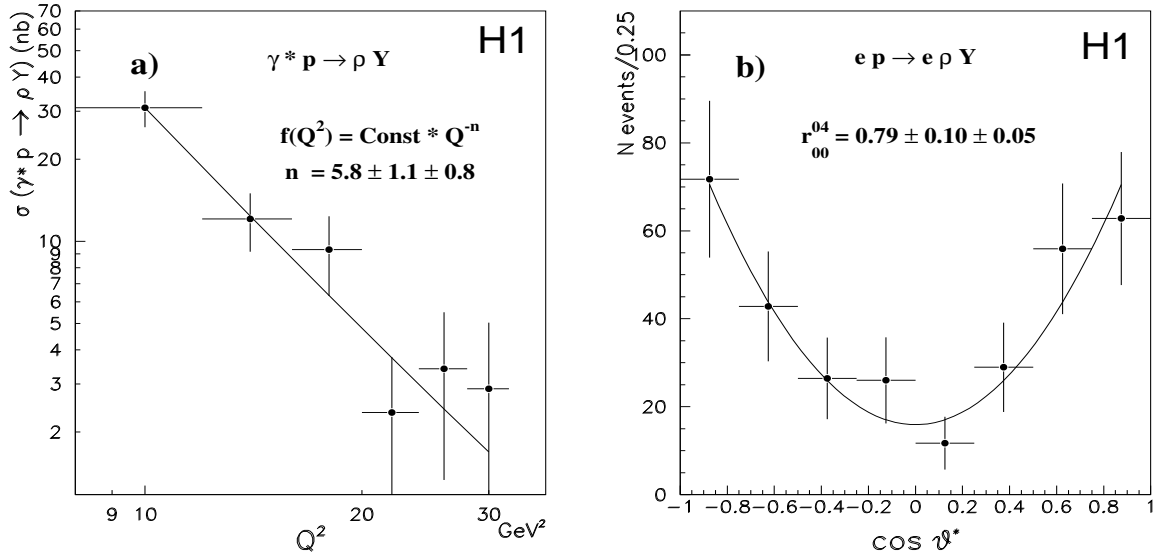
Figure 3: a) Q^2 distribution of the proton dissociative ρ meson production $\gamma^* p$ cross section after efficiency correction. The solid curve represents a fit with the Q^{-n} function, the backgrounds being taken into account in the fit procedure. b) Efficiency corrected $\cos\vartheta^*$ distribution, the backgrounds being subtracted in the fit. Only statistical errors are presented for both distributions.

angular distribution can be expressed in terms of the appropriate ρ meson spin density matrix element r_{00}^{04} as:

$$\frac{\mathrm{d}N}{\mathrm{d}\cos\vartheta^*} \propto 1 - r_{00}^{04} + (3\ r_{00}^{04} - 1)\ \cos^2\vartheta^*, \qquad (7)$$

where r_{00}^{04} is the probability for the ρ meson to be longitudinally polarised.

The acceptance corrected $\cos\vartheta^*$ angular distribution is shown in Fig. 3b. The backgrounds are subtracted in the fit procedure. A flat distribution is assumed for DD and DIS and the value $r_{00}^{04} = 0.73 \pm 0.05 \pm 0.02$ (see [7]) is used for the elastic scattering background subtraction. The fit yields $r_{00}^{04} = 0.79 \pm 0.10 \pm 0.05$, again similar to the elastic scattering data value [7] and indicating that the ρ mesons are mostly longitudinally polarised also for the proton dissociative process. The systematic uncertainties are mostly due to the uncertainties of the background subtraction and the fit procedure.

3.6   Test of the Factorisation Hypothesis

The results obtained for $\gamma^* p$ elastic scattering can be compared with other diffractive processes in the framework of the factorisation hypothesis using eq. (1). For example, in the case of proton-proton collisions the coupling constant $g_{\gamma^*\rho}$ is replaced by g_{pp}, which cancels in the ratio.

Assuming an exponential $|t|$ dependence of the elastic and proton dissociative processes

and a universal M_Y dependence of proton dissociation [5], eq. (1) leads after integration over a fixed M_Y interval to:

$$\frac{\mathrm{d}\sigma_{pdis}/\mathrm{d}t(t=0)}{\mathrm{d}\sigma_{el}/\mathrm{d}t(t=0)} = \frac{\sigma_{pdis}b_{pdis}}{\sigma_{el}b_{el}} = f_1, \qquad b_{el} - b_{pdis} = f_2, \qquad (8)$$

where σ_{el} and σ_{pdis} are the elastic and proton dissociative cross sections integrated over t and M_Y.

If factorisation holds, f_1 and f_2 are expected to be the same in different diffractive processes. Table 3 compares the values for f_1 and f_2 in $\gamma^{(*)}p$ and pp interactions, albeit with somewhat different centre of mass energies. Such energy variations are not expected to affect this comparison. Note that after efficiency corrections similar $M_Y^2/W^2 < 0.05$ regions are used in the measurements.

Experiment	ISR, $pp \to pY$ [17]	H1, $\gamma^*p \to \rho Y$	H1, $\gamma p \to J/\psi Y$ [2]
cms energy, GeV	53	60 - 180	30 - 150
b_{el}, GeV^{-2}	13.1 ± 0.3	7.0 ± 1.0	4.0 ± 0.3
b_{pdis}, GeV^{-2}	6.5 ± 1.0	2.1 ± 0.7	1.6 ± 0.3
$\sigma_{pdis}/\sigma_{el}$	0.48 ± 0.03	0.66 ± 0.17	1.0 ± 0.2
f_1	0.24 ± 0.04	0.20 ± 0.09	0.40 ± 0.11
f_2, GeV^{-2}	6.6 ± 1.0	4.9 ± 1.2	2.4 ± 0.4

Table 3: Comparison of the f_1 and f_2 values for $\gamma^{(*)}p$ and pp collisions.

It is observed that the ρ meson data with $Q^2 > 7$ GeV^2 are consistent within errors with the proton-proton results from the ISR [17], whereas the f_1 and f_2 values obtained in J/ψ photoproduction [2] are somewhat different.

4 Elastic Electroproduction of ϕ Mesons

4.1 Energy Dependence of Vector Meson Production

Contrasting results are obtained for the W dependence of the cross sections for elastic production of different vector mesons and at different photon virtualities. On the one hand, high energy ρ meson production by quasi-real photons exhibits behaviour typical of hadronic interactions, in particular a slow increase of the cross section with energy: $\sigma\,(\gamma p \to \rho p) \propto (W^2)^{2\epsilon}$, where $\epsilon \approx 0.08$ (at $|t| = 0$ GeV^2) [45], and shrinkage of the diffraction peak, i.e. an increase of the b slope with increasing energy. It is therefore attributed essentially to soft pomeron exchange, dominated by QCD non-perturbative features. On the other hand, the cross section for photoproduction of J/ψ mesons [2,6]

---

[5]Both assumptions are in a good agreement with the experimental data for the low $|t|$ region and possible differences between the M_Y dependences of the pp and γ^*p processes due to the variation of the b-slopes with M_Y are expected to be inside the theoretical and experimental uncertainties.

increases much faster with energy ($\epsilon \approx 0.25$), as qualitatively expected in models in which the large mass of the charm quark provides a hard scale for perturbative QCD and the pomeron is interpreted as a two gluon exchange. At higher photon virtualities, $Q^2 \gtrsim 8$ GeV^2, measurements of ρ production [7,8] indicate a steeper rise of the cross section with energy, indicative of a transition regime between soft and hard processes, whereas the behaviour of the J/ψ cross section is similar to that of photoproduction [7].

It is thus interesting to study the electroproduction of ϕ mesons, which have a mass between those of the ρ and J/ψ mesons, and presumably a more compact wave function than the ρ meson. Moreover, ϕ meson production is "OZI" exotic [46] in both the s and t channels and is thus dominated by pomeron exchange.

The photoproduction of ϕ mesons [5,20,47] exhibits features typical of soft diffractive interactions, similar to the ρ case. It is of particular interest to study the ϕ/ρ cross section ratio evolution with Q^2 and W. This ratio is measured in photoproduction to be well below the value 2/9 expected from quark charge counting and SU(3) symmetry. Both in the soft pomeron and in the perturbative QCD approaches [30,31] the ratio increases with Q^2, and in the latter case exceeds the value 2/9 at high Q^2.

The only existing results on ϕ meson electroproduction for $Q^2 \gtrsim 6$ GeV^2 are from the EMC [13] and NMC [12] Collaborations at $\langle W \rangle \approx 14$ GeV and the ZEUS Collaboration [9] at HERA [6].

4.2 ep and $\gamma^* p$ Cross Sections

The production of ϕ mesons is studied in the kinematic region

$$6 < Q^2 < 20 \text{ GeV}^2, \quad 0.02 < y < 0.2 . \tag{9}$$

These cuts are equivalent to $42 < W < 134$ GeV. In addition to the selection criteria presented in section 2, the following cuts are applied to select the elastic ϕ sample:

$$P_t^2 < 0.6 \text{ GeV}^2, \quad \sum (E - P_z) > 45 \text{ GeV} , \tag{10}$$

where the sum runs over the measured energy and momentum of the kaons from the ϕ meson decay and the scattered positron. These cuts suppress non-diffractive backgrounds and reduce radiative corrections respectively.

Fig. 4 shows the invariant $K^+ K^-$ mass distribution for the events passing all selection criteria, the kaon mass having been assigned to the detected particles in the central tracking detector. A clear ϕ signal over little background is observed in the mass region $1.00 < M_{K^+ K^-} < 1.04$ GeV/c^2, which contains 29 events. The curve superimposed on Fig. 4 is the result of a fit to a relativistic Breit-Wigner distribution with a width fixed at the nominal value [44], convoluted with a Gaussian distribution, over a linear background starting at threshold ($M = 2 M_K$). The r.m.s. width of the Gaussian distribution, which reflects the detector resolution, is fixed at a value of 4.5 MeV/c^2 as obtained from MC. Here, as in the ρ analysis, the program DIFFVM [41] is used for MC simulation. The

---

[6] The electroproduction of ϕ mesons at $Q^2 \lesssim 2.5$ GeV^2 has also been measured in fixed target experiments for $W < 4$ GeV [48] and for $W \approx 12$ GeV [49].
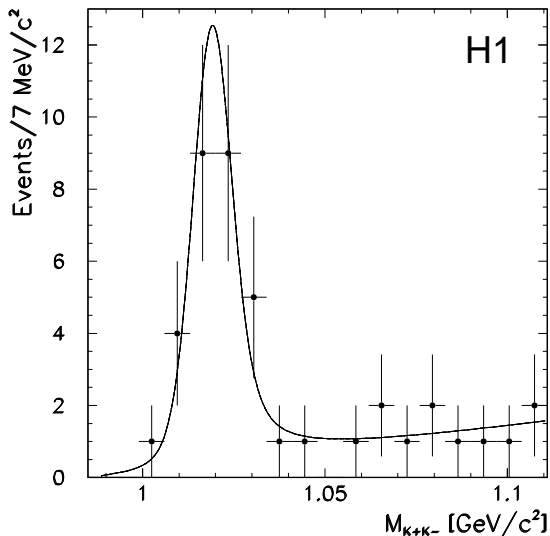
Figure 4: $M_{K^+K^-}$ invariant mass distribution for the selected events; the curve is the result of a fit to a Breit-Wigner distribution convoluted with a Gaussian, over a linear background.

fitted mass of the ϕ meson is 1019 ± 2 MeV/c^2, in good agreement with the nominal value of 1019.4 MeV/c^2.

The non-ϕ background under the signal in the mass region $1.00 < M_{K^+K^-} < 1.04$ GeV/c^2 is estimated to be $6 \pm 4\%$. The error includes statistical and systematic uncertainties estimated by varying the shape of the background and the limits of the fit. Because of the limited statistics, which do not allow an independent estimate, the background due to diffractive ϕ production with proton dissociation is taken to be the same as for the ρ analysis, i.e. $9 \pm 8\%$ of the selected signal, as would be expected with a factorisation of the diffractive vertex.

After background subtraction and corrections for efficiencies and acceptances, for QED radiation effects and for the known ϕ decay branching ratio into a K^+K^- pair, the ep cross section for elastic ϕ production is

$$\sigma(ep \rightarrow e\phi\,p) = 50.7 \pm 11.8 \text{ (stat.)} \pm 6.4 \text{ (syst.) pb,}$$

integrated over the range $6 < Q^2 < 20$ GeV^2 and $42 < W < 134$ GeV.

The ep cross sections are converted into γ^*p cross sections using a relation similar to eq. (6). Uncertainties in the Q^2 and W dependences measured in the present data lead to systematic errors included in the quoted results.

The γ^*p cross section for ϕ meson elastic production, measured at $\langle W \rangle \approx 100$ GeV, is

$$\sigma(\gamma^*p \rightarrow \phi\,p) = 9.6 \pm 2.4 \text{ nb} \quad \text{at } \langle Q^2 \rangle = 8.3 \text{ GeV}^2,$$

$$\sigma(\gamma^*p \rightarrow \phi\,p) = 3.1 \pm 1.0 \text{ nb} \quad \text{at } \langle Q^2 \rangle = 14.6 \text{ GeV}^2.$$

The quoted errors are the quadratic sums of the statistical and the systematic uncertainties.

These results are presented in Fig. 5, together with a compilation of photoproduction and leptoproduction results [5, 9, 12, 20, 47, 48, 50] as a function of W. The NMC measurements were scaled to the values $Q^2 = 2.1$, 8.3 and 14.6 GeV^2 using their measured Q^2 dependence and the relevant values of the polarisation parameter ε; the ZEUS measurements are made at Q^2 values very close to ours. The overall normalisation uncertainties of 25 % for the results of Cassel et al. [48], 20 % for NMC [12] and 32 % for ZEUS [9] are not shown on the plot.

The cross section for elastic photoproduction of ϕ mesons shows only a slow rise from the fixed target to the HERA energies, consistent with soft pomeron exchange. In contrast, at higher Q^2, the HERA values of the cross sections are significantly larger than those of the NMC experiment, although the errors are large and the comparison involves two different experiments.
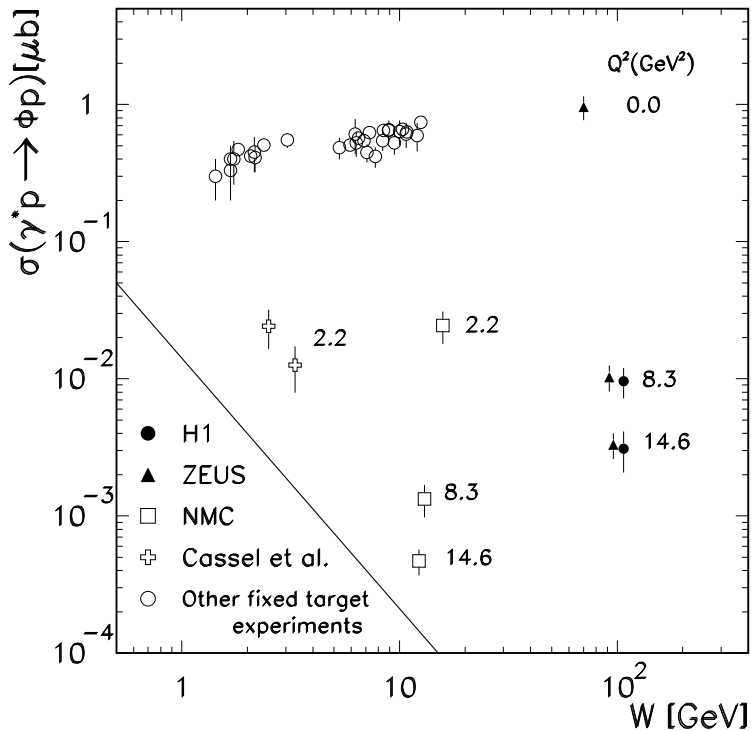

Figure 5: Cross section for $\gamma^* p \rightarrow \phi p$ as a function of W for several values of Q^2 (GeV^2). The overall normalisation uncertainties of 25% for the results of Cassel et al., 20% for NMC and 32% for ZEUS are not included. The H1 errors are the quadratic sums of the statistical and the systematic uncertainties.

4.3 Q^2 and P_t^2 Dependences and Polarisation

The Q^2 dependence of the total $\gamma^* p$ cross section for elastic ϕ production (see Fig. 6a) can be described by the form Q^{-n} with $n = 4.0 \pm 1.5 \pm 0.6$, where the first error is statistical and the second reflects the uncertainty on the background contribution and

the spread of results according to the details of the fitting procedure. This value is close to that obtained by the NMC Collaboration [12], with $n = 4.5 \pm 0.8$, and by the ZEUS Collaboration [9], with $n = 4.1 \pm 1.2$ (stat.). It is also similar to that measured for the ρ ($n = 5.0 \pm 1.0 \pm 0.4$ [7]).
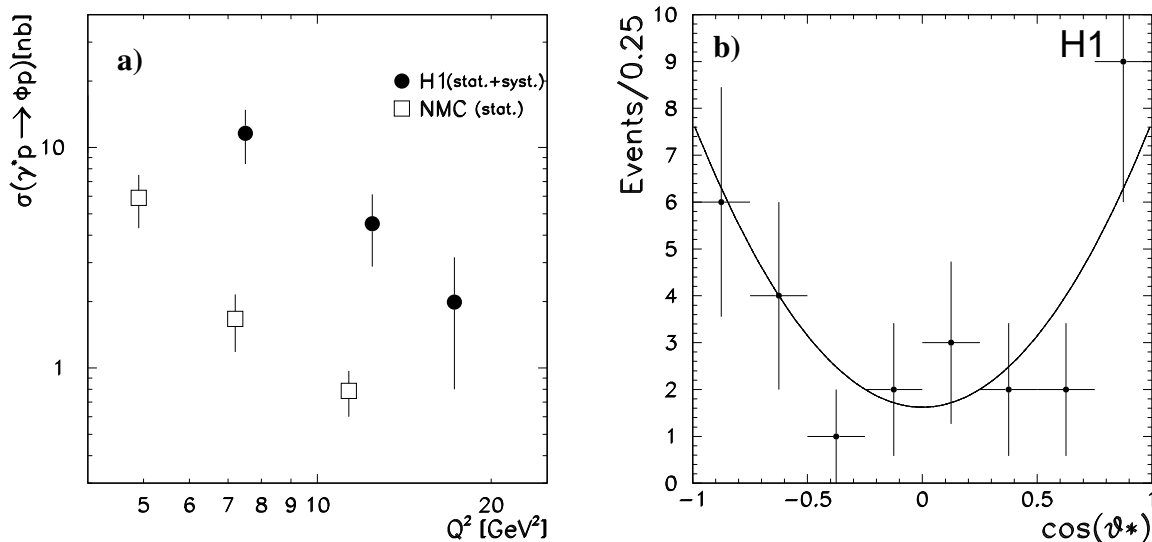

Figure 6: a) Q^2 dependence of the $\gamma^* p \rightarrow \phi p$ cross section. b) Distribution of $\cos \vartheta^*$ for the selected ϕ events; the backgrounds are taken into account in the fit. Only the statistical errors are shown.

An exponential fit to the P_t^2 distribution for $P_t^2 < 0.6$ GeV^2 gives for the slope the value $b = 5.2 \pm 1.6$ (stat.) ± 1.0 (syst.) GeV^{-2}. The result is corrected for the presence of the two backgrounds mentioned above, with fixed relative contributions with respect to the elastic signal and with fixed slopes. The slope of the proton dissociation background is assumed to be $b = 2.0 \pm 1.0$ GeV^{-2} (no dependence of the slope on the proton excitation mass is assumed) and the slope for the non-resonant background is taken to be $b = 0.4 \pm 0.4$ GeV^{-2}, as obtained from a fit to the P_t^2 distribution of the events with $1.05 < M_{K^+ K^-} < 1.3$ GeV/c^2 and which do not belong to the ρ peak ($M_{\pi^+ \pi^-} < 0.4$ GeV/c^2). The systematic error includes the effects of varying the amount of each background and its slope within uncertainties, and those of changing the details of the fitting procedure.

As for the ρ, the acceptance corrected distribution of $\cos \vartheta^*$ allows the extraction of the parameter r_{00}^{04} (see Fig. 6b). After subtraction of the non-resonant background, which is consistent with being flat in $\cos \vartheta^*$, and correction for detector effects, the fit gives $r_{00}^{04} = 0.77 \pm 0.13 \pm 0.02$, where the first error is statistical, and the second reflects the uncertainty on the background subtraction. This result is close to that obtained for elastic and proton dissociative ρ production. Thus elastically electroproduced ϕ mesons are observed to be mostly longitudinally polarised, in agreement with model predictions [23, 30].

4.4 Cross Section Ratio $\sigma(\phi)/\sigma(\rho)$

The study of the Q^2 and W evolutions of the ϕ/ρ cross section ratio for elastic production is of particular interest. Systematic uncertainties largely cancel in the ratio as the same selection criteria are used for the two event samples. It is thus possible to relax the requirements on the positron cluster position and energy deposition in the BEMC, and those on the associated BPC hit, since the trigger conditions and the kinematic variable reconstruction are affected in the same way for both samples. The accepted kinematic domain is then extended to $5 < Q^2 < 20$ GeV^2. A slight difference in the acceptances for the two samples, due to the different opening angles in the laboratory system between the two decay hadrons, is taken into account.

After acceptance corrections and background subtraction, the ϕ to ρ cross section ratio $R_{\phi/\rho}$ is measured to be

$$R_{\phi/\rho} = 0.18 \pm 0.03 \quad \text{at } \langle Q^2 \rangle = 6.1 \text{ GeV}^2 \quad (5 < Q^2 < 8.3 \text{ GeV}^2),$$

$$R_{\phi/\rho} = 0.19 \pm 0.04 \quad \text{at } \langle Q^2 \rangle = 12.0 \text{ GeV}^2 \quad (8.3 < Q^2 < 20 \text{ GeV}^2),$$

for $\langle W \rangle \approx 100$ GeV. These results are presented in Fig. 7, together with the high Q^2 results of the EMC [13], NMC [12] and ZEUS Collaborations [9], and with the ZEUS photoproduction measurement [5].
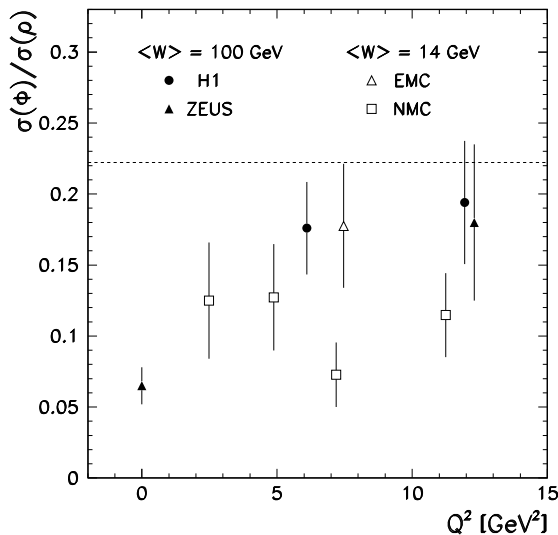

Figure 7: Ratio of the cross sections for elastic ϕ and ρ production, as a function of Q^2. The H1 and ZEUS (at $Q^2 \approx 12.3$ GeV^2) errors are the quadratic sums of the statistical and systematic uncertainties. For the EMC, NMC and ZEUS (at $Q^2 \approx 0$ GeV^2) points only statistical errors are shown. The overall normalisation uncertainties of about 10 % for the NMC and EMC results are not included. The dashed line corresponds to the ratio 2/9 from quark charge counting and SU(3).

The cross section ratio values from HERA at high Q^2 are close to the SU(3) quark charge counting prediction of 2/9, in contrast with photoproduction results ($R_{\phi/\rho} \simeq 0.07$).

Approaches based on perturbative QCD predict that this value for the ratio should be exceeded at very large Q^2 [30,31]. In Fig. 7 there is also an indication that, for comparable Q^2 values, the ratio $R_{\phi/\rho}$ may be higher at HERA than for the fixed target experiments.

5 Summary

The electroproduction of ρ mesons with proton diffractive dissociation has been studied at HERA with the H1 detector. The ratio of the proton dissociative to the elastic cross section is measured to be $\sigma(\gamma^*p \to \rho Y)/\sigma(\gamma^*p \to \rho p) = 0.65 \pm 0.11 \pm 0.13$, in the kinematic range $7 < Q^2 < 35\,\mathrm{GeV}^2$ and $60 < W < 180\,\mathrm{GeV}$ (corresponding to $\langle Q^2 \rangle \approx 10$ GeV^2 and $\langle W \rangle \approx 128$ GeV) for the mass interval $M_Y^2/W^2 < 0.05$. Dividing the kinematic range into two W and two Q^2 intervals gives no significant indication of variation of this ratio.

The exponential slope of the P_t^2 distribution for proton dissociative ρ meson electroproduction is found to be $b_{pdis} = 2.1 \pm 0.5 \pm 0.5$ GeV^{-2}, with no significant M_Y dependence. The Q^2 distribution for the $\gamma^*p \to \rho Y$ process is well fitted by the form Q^{-n}, with $n = 5.8 \pm 1.1 \pm 0.8$, similar to the value $n = 5.0 \pm 1.0 \pm 0.4$ for elastic ρ production. The probability r_{00}^{04} for the ρ meson to be longitudinally polarised is measured to be $r_{00}^{04} = 0.79 \pm 0.10 \pm 0.05$, close to the value $r_{00}^{04} = 0.73 \pm 0.05 \pm 0.02$ for elastic ρ production, demonstrating that ρ mesons are mostly longitudinally polarised also in the proton dissociative process.

The similarity of the Q^2 and polarisation behaviour for ρ meson electroproduction in proton dissociative and in elastic scattering, and the comparison of these results with proton-proton collider results, do not provide any evidence of correlations between the processes originating from different vertices, i.e. for breaking of factorisation.

The cross section for the elastic electroproduction of ϕ mesons has been measured at HERA in the kinematic range $6 < Q^2 < 20$ GeV^2 and $42 < W < 134$ GeV. At this Q^2 the cross section is significantly larger than observed in the fixed target measurement [12] at smaller W, in contrast to the photoproduction case. The Q^2 dependence of the γ^*p cross section is well described by the form Q^{-n} with $n = 4.0 \pm 1.5 \pm 0.3$. The exponential slope of the P_t^2 distribution is found to be $b = 5.2 \pm 1.6 \pm 1.0$ GeV^{-2}. Elastically electroproduced ϕ mesons are found to be mostly longitudinally polarised.

The ratio of the cross sections for elastic electroproduction of ϕ and ρ mesons is measured, for $5 < Q^2 < 20$ GeV^2, to be $R_{\phi/\rho} = 0.18 \pm 0.03$. This ratio is significantly larger than in photoproduction, and the comparison with fixed target results provides some indication that, for comparable Q^2 values, the ratio is may be higher at HERA than at lower energy.

Acknowledgments

directorate for the hospitality which they extend to the non–DESY members of the collaboration. We further thank A.B. Kaidalov, L.L. Frankfurt and E.M. Levin for useful discussions.

References

[1] S. Aid et al., H1 Coll., *Nucl. Phys.* **B463** (1996) 3.

[2] S. Aid et al., H1 Coll., *Nucl. Phys.* **B472** (1996) 3.

[3] M. Derrick et al., ZEUS Coll., *Zeit. Phys.* **C69** (1995) 39;
    M. Derrick et al., ZEUS Coll., preprint DESY-96-183 (1996).

[4] M. Derrick et al., ZEUS Coll., *Zeit. Phys.* **C73** (1996) 73.

[5] M. Derrick et al., ZEUS Coll., *Phys. Lett.* **B377** (1996) 259.

[6] M. Derrick et al., ZEUS Coll., *Phys. Lett.* **B350** (1995) 120.

[7] S. Aid et al., H1 Coll., *Nucl. Phys.* **B468** (1996) 3.

[8] M. Derrick et al., ZEUS Coll., *Phys. Lett.* **B356** (1995) 601.

[9] M. Derrick et al., ZEUS Coll., *Phys. Lett.* **B380** (1996) 220.

[10] R.M. Egloff et al., *Phys. Rev. Lett.* **43** (1979) 657;
    D. Aston et al., *Nucl. Phys.* **B209** (1982) 56.

[11] U. Camerini et al., *Phys. Rev. Lett.* **35** (1975) 483;
    M. Binkley et al., *Phys. Rev. Lett.* **48** (1982) 73;
    B.H. Denby et al., *Phys. Rev. Lett.* **52** (1984) 795;
    R. Barate et al., *Zeit. Phys.* **C33** (1987) 505;
    P.L. Frabetti et al., *Phys. Lett.* **B316** (1993) 197.

[12] M. Arneodo et al., NMC Coll., *Nucl. Phys.* **B429** (1994) 503.

[13] J. Ashman et al., EMC Coll., *Zeit. Phys.* **C39** (1988) 169.

[14] F. Abe et al., CDF Coll., *Phys. Rev.* **D50** (1994) 5518;
    F. Abe et al., CDF Coll., *Phys. Rev.* **D50** (1994) 5535.

[15] M. Bozzo et al., UA4 Coll., *Phys. Lett.* **B147** (1984) 392;
    D. Bernard et al., UA4 Coll., *Phys. Lett.* **B186** (1987) 227.

[16] R.E. Ansorge et al., UA5 Coll., *Zeit. Phys.* **C33** (1986) 175.

[17] J.C.M. Armitage et al., CHLM Coll., *Nucl. Phys.* **B194** (1982) 365;
    N. Amos et al., *Phys. Lett.* **B120** (1983) 460.

[18] P.D.B. Collins, *An Introduction to Regge Theory and High-Energy Physics*, Cambridge University Press, Cambridge, England, 1977.

[19] J.J. Sakurai, *Phys. Rev. Lett.* **22** (1969) 981;
J.J. Sakurai and D. Schildknecht, *Phys. Lett.* **B40** (1972) 121.

[20] T.H. Bauer et al., *Rev. Mod. Phys.* **50** (1978) 261, and references therein.

[21] F.E. Low, *Phys. Rev.* **D12** (1975) 163;
S. Nussinov, *Phys. Rev. Lett.* **34** (1975) 1268.

[22] A. Donnachie and P.V. Landshoff, *Phys. Lett.* **B348** (1995) 213.

[23] J.R. Cudell, *Nucl. Phys.* **B336** (1990) 1.

[24] M.G. Ryskin, *Zeit. Phys.* **C57** (1993) 89.

[25] B.Z. Kopeliovich et al., *Phys. Lett.* **B324** (1994) 469;
N.N. Nikolaev, B.G. Zakharov and V.R. Zoller *Phys. Lett.* **B366** (1996) 337;
J. Nemchik et al., *Phys. Lett.* **B374** (1996) 199.

[26] L.P.A. Haakman, A. Kaidalov and J.H. Koch, *Phys. Lett.* **B365** (1996) 411.

[27] I.F. Ginzburg and D.Yu. Ivanov, preprint hep-ph/9604437 (1996).

[28] S.J. Brodsky et al., *Phys. Rev.* **D50** (1994) 3134.

[29] E. Gotsman, E.M. Levin and U. Maor, *Nucl. Phys.* **B464** (1996) 251.

[30] L. Frankfurt, W. Koepf and M. Strikman, *Phys. Rev.* **D54** (1996) 3194.

[31] J. Nemchick et al., preprint DFTT 71/95, KFA-IKP(TH)-24-95,hep-ph/9605231 (1996).

[32] I. Abt et al., H1 Coll., *The H1 detector at HERA, Nucl. Instr. Meth.* **A386** (1997) 310, 348.

[33] S. Bentvelsen, J. Engelen and P. Kooijman, Proc. of the Workshop on Physics at HERA, ed. W. Buchmüller and G. Ingelman, Hamburg 1992, Vol. 1, p. 23;
K.C. Hoeger, ibid., p.43;
G. Wolf, preprint DESY-94-022 (1994).

[34] A.B. Kaidalov, *Phys. Rep.* **50** (1979) 157.

[35] K. Goulianos, *Phys. Rep.* **101** (1983) 169.

[36] H. Holtmann at al., *Zeit. Phys.* **C69** (1996) 297.

[37] A. Donnachie and P.V. Landshoff, *Nucl. Phys.* **B231** (1984) 189.

[38] D.S. Ayres et al., *Phys. Rev. Lett.* **37** (1976) 1724.

[39] S.P. Misra, A.R. Panda and B.K. Parida, *Phys. Rev.* **D22** (1980) 1574.

[40] C. Conta et al., *Nucl. Phys.* **B175** (1980) 97.

[41] B. List, *DIFFVM program, Diploma Thesis*, Techn. Univ. Berlin, unpubl. (1993).

[42] H. Spiesberger, *HERACLES* 4.4, unpublished program manual (1993);
A. Kwiatkowski, H. Spiesberger and H.-J. Möhring, Proc. of the Workshop on Physics at HERA, ed. W. Buchmüller and G. Ingelman, Hamburg 1992, Vol. 3, p. 1294.

[43] J.D. Jackson, *Nuovo Cim.* **34** (1964) 1644.

[44] R.M. Barnett et al., *Review of Particle Physics, Phys. Rev.* **D54** (1996) 1.

[45] A. Donnachie and P.V. Landshoff, *Phys. Lett.* **B296** (1992) 227.

[46] S. Okubo, *Phys. Lett.* **5** (1963) 165;
G. Zweig, CERN Reports TH-401, TH-412 (1964);
J. Iizuka, *Prog. Theor. Phys. Suppl.* **37/38** (1966) 21.

[47] R.M. Egloff et al., *Phys. Rev. Lett.* **43** (1979) 657;
J. Busenitz et al., *Phys. Rev.* **D40** (1989) 1.

[48] D.G. Cassel et al., *Phys. Rev.* **D24** (1981) 2787.

[49] W.D. Shambroom et al., CHIO Coll., *Phys. Rev.* **D26** (1982) 1.

[50] S.I. Alekhin et al., CERN-HERA 87-01(1987), ed. H. Schopper in: Landolt-Bornstein, New Series, Vol. 12b.